Carbon Nanotube−Confined Evolution of Co−Ni Alloy Nanowires with High-Density Lamellar Twin Boundaries

ARTICLE *in* THE JOURNAL OF PHYSICAL CHEMISTRY C · OCTOBER 2008

Impact Factor: 4.77 · DOI: 10.1021/jp804380x

6 AUTHORS, INCLUDING:

Shouai Feng
Chinese Academy of Sciences
10 PUBLICATIONS **150** CITATIONS
SEE PROFILE

Jianghong Zhao
Chinese Academy of Sciences
54 PUBLICATIONS **905** CITATIONS
SEE PROFILE

Zhenping Zhu
Chinese Academy of Sciences
192 PUBLICATIONS **11,012** CITATIONS
SEE PROFILE

Carbon Nanotube-Confined Evolution of Co−Ni Alloy Nanowires with High-Density Lamellar Twin Boundaries

Shouai Feng, Jianghong Zhao, Guixiang Du, Chang Song, Jinling Song, and Zhenping Zhu*

State Key Laboratory of Coal Conversion, Institute of Coal Chemistry, Chinese Academy of Sciences, Taiyuan 030001, People's Republic of China

Received: May 18, 2008; Revised Manuscript Received: July 28, 2008

Co−Ni alloy nanowires were in situ sheathed inside carbon nanotubes by a detonation-assisted chemical vapor deposition. The nanowires exhibit an unusual high-density lamellar-twinned structure. The observations of the frozen intermediates suggested that the nanowires form from a fusion of small alloy particles. The formation of the unusual high-density lamellar-twinned structures is associated with a confinement effect of the closed narrow channels of carbon nanotubes. Within the channels, the fusion of Co−Ni alloy particles proceeds in a unique kinetic environment, in which high-density lamellar twinning boundaries are formed to meet a quick reduction of excess energy.

1. Introduction

Inorganic nanowires have drawn increasing interest due to their unique physical properties and wide potential applications in nanometer-scale electronic[1,2] and optoelectronic devices,[3] sensors,[4] and magnetic recording devices.[5,6] The growth or evolution of the nanowires is normally driven kinetically due to the intrinsic meta-stability of the nanostructures. In the kinetic processes, structural defects, including twin boundaries, are frequently introduced into the nanowires. The presence of the twin boundaries often limits the performances of the materials.[3] On the other hand, twin boundaries can act as obstacles to restrict lattice dislocation movements so that the strength of a solid is improved.[7−9] More interestingly, Lu et al.[10] recently reported that the introduction of high-density lamellar twin boundaries not only enhances copper strength but also effectively retains its electrical conductivity, which provides a potential solution to the inconsistency between mechanical strength and electrical conductivity involved in conventional metallic solids. Furthermore, theoretical calculations indicate that diamond-type and blende-type semiconductors with coherent twinned structures have unique properties, such as small band gaps and direct optical transitions, different from bulk semiconductor counterparts.[11,12]

It has been known that because twin plane energy is about one-half the conventional stacking fault energy,[13] the formation of twinned structures is thermodynamically beneficial to the reduction of the excess interfacial energy.[10] On the other hand, as compared to the nucleation of ordinary crystal planes, the formation of twin planes is less energetically favored,[3] and thus driven kinetically, greatly depending on the employed conditions and local environments.[10,14] The twins existing in inorganic nanowires mainly exhibit two types of structures: cyclic twins and lamellar twins. From the reported results, cyclic twins with 5-fold symmetry are often formed in metal nanowires, for example, gold,[15] copper,[16] and silver[17−21] nanowires, while lamellar twins with high density are frequently observed in the nanowires made of various semiconductor materials such as GaP,[3,12] InP,[22,23] ZnS,[24] ZnSe,[25] and Zn_2SnO_4.[26] It remains a significant challenge to synthesize high-density lamellar twins in metal nanowires, although sparse lamellar twin segments have been observed in gold,[8,27] copper,[28,29] and silver[30] nanowires.

Here, we report that during the evolution of carbon nanotubes (CNTs), an in situ formation of metallic Co−Ni alloy nanowires inside CNTs (Co−Ni@CNTs) results in an unusual lamellar twined structure with high-density twin boundaries. The formation of the twinned structures is associated with a confinement effect of the closed narrow channels of CNTs. Within the channels, the coalescence of Co−Ni alloy particles proceeds in a unique confined kinetic environment, in which high-density lamellar twinning boundaries are formed to quickly reduce excess energy.

2. Experimental Methods

In Situ Sheathing Co−Ni Alloy Nanowires Inside CNTs. Co−Ni alloy nanowires were in situ sheathed inside CNTs during the CNT synthesis, using the previously reported detonation-assisted chemical vapor deposition (DACVD).[31−33] The detailed experimental processes were similar to those described elsewhere.[31,34] To obtain CNT-sheathed Co−Ni alloy nanowires, a detonation recipe containing picric acid, cobalt acetate ($Co(AC)_2 \cdot 4H_2O$), nickel formate ($Ni(CHOO)_2 \cdot 2H_2O$), and cyclohexane was employed. Before the experiment, the start materials were physically mixed in desired ratios (typically 20:1:1:3 in molar ratio). The detonation experiments were performed in a sealed stainless steel pressure vessel (15 cm^3 of volume), with 3.5 g of the mixture. The detonation was induced by external heating (15 °C/min) to 310 °C (the exploding temperature of picric acid). After the detonation, the vessel was cooled in air to ambient temperature. The gaseous products were vented, and the solid products were collected for further characterizations.

Freezing Formation Process at Intermediary Stages. To obtain intermediate objects during the formation of CNT-sheathed Co−Ni alloy nanowires, a freezing operation was carried out. After the detonation, the reaction vessel was instantly taken out from the heating furnace, and the majority of the produced hot gases was released immediately, within 10 s typically, from initial 20 to 6 MPa. Such an operation effectively reduced the system temperature and froze the formation at intermediary stages. After the operation, the vessel was cooled

* Corresponding author. E-mail: zpzhu@sxicc.ac.cn.

10.1021/jp804380x CCC: $40.75
Published on Web 09/04/2008

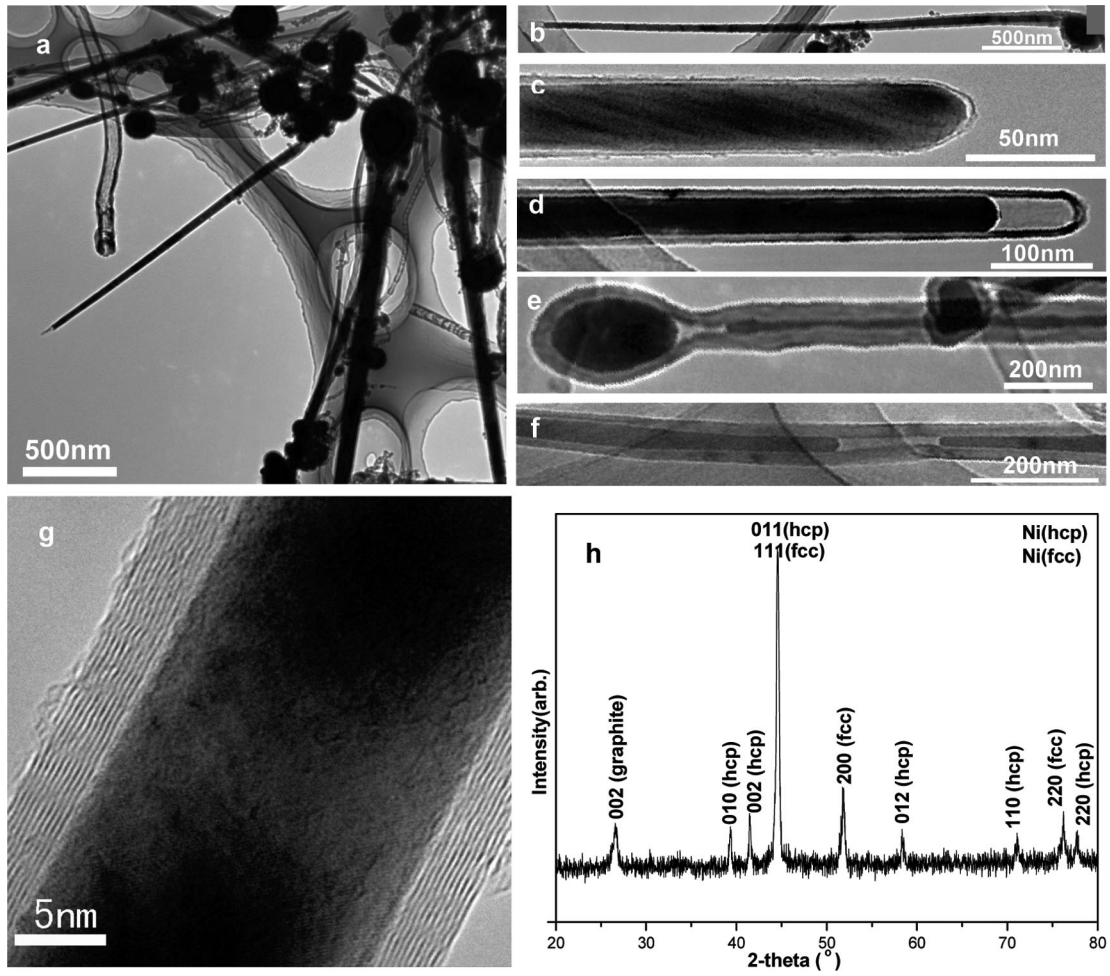

Figure 1. (a−f) TEM image of the produced Co−Ni@CNTs. (g) The carbon-focused HRTEM image of an individual Co−Ni@CNT. (h) XRD pattern of the products.

to room temperature naturally, the remained gases were vented, and the solid products were collected for further characterization.

Electron Microscopic, X-ray, and Element Analyses. The as-synthesized materials were characterized by transmission electron microscopy (TEM, JEOL JEM-2010), using an accelerating voltage of 200 kV. The microscopy was equipped with an energy dispersive X-ray spectrometer (EDX) for elemental analysis. Before being analyzed, the samples were prepared by sonicating in ethanol for 10 min, followed by depositing one drop of the resulted suspension on thin carbon film supported on holey copper grid. Real-time observation of the fusion action of Co−Ni alloy nanoparticles under electronic beam irradiation was carried out in the HRTEM. The electron irradiation intensity was in the range of 30−50 A/cm^2. The vacuum was better than 10^{-5} Pa. The X-ray diffraction (XRD) patterns of the samples were obtained on a powder X-ray diffractometer (D8 ADVANCE BRUKER) using Cu Ka radiation (λ = 1.5406 Å). The contents of metals in the products were determined by inductively coupled plasma spectrometry (ICP, Atomscan 16, TJA).

3. Results and Discussion

For the CNT synthesis by DACVD method, the molar ratio of metal to carbon in start materials was normally controlled in the range of 1:50−100 (excluding the carbons involved in picric acid, which mostly transformed into gaseous production during the detonation). Under the conditions, the detonation reactions result in high-yield CNTs with hollow channels.[33] In the present experiments for the production of Co−Ni@CNTs, cobalt acetate and nickel formate are employed as combined catalysts, and the molar ratio of total metal to carbon is 1:9, much larger than that in the synthesis of hollow CNTs. The reaction system with high content of metal effectively produced metal nanowires sheathed inside CNTs (Figure 1a), which is about 45% of the products, based on the total observations by transmission electron microscopy (TEM). They have length of up to 10 μm (Figure S1) and exhibit pinlike morphology, with thick ends of up to 300 nm in diameter and thin ends of down to 10 nm. Interestingly, the coexisting hollow CNTs are uniform in diameter from one end to the other end (Figure S2), suggesting that the formation of the pinlike metal nanaowire-sheathed CNTs is associated with the encapsulation of the metals, although it is still unclear about the mechanism. In the majority of the metal nanowire-sheathed CNTs, the metal nanowires are continuously filled inside the channels of CNTs along the whole tube length (Figures 1a−c and S1), but small spaces are presented for some cases (Figure 1d−f). Carbon-shell-focused high-resolution TEM images show that the tube walls are well crystallized (Figure 1g).

Elemental analyses by energy dispersive X-ray spectrometer (EDX) indicate that the sheathed metal nanowires consist of Co and Ni, along the whole lengths of them (Figure S3). The atomic ratio of Co to Ni is about 8:7, close to the ICP element analysis results (Co 18.1 wt % and Ni 16.3 wt %) and the value

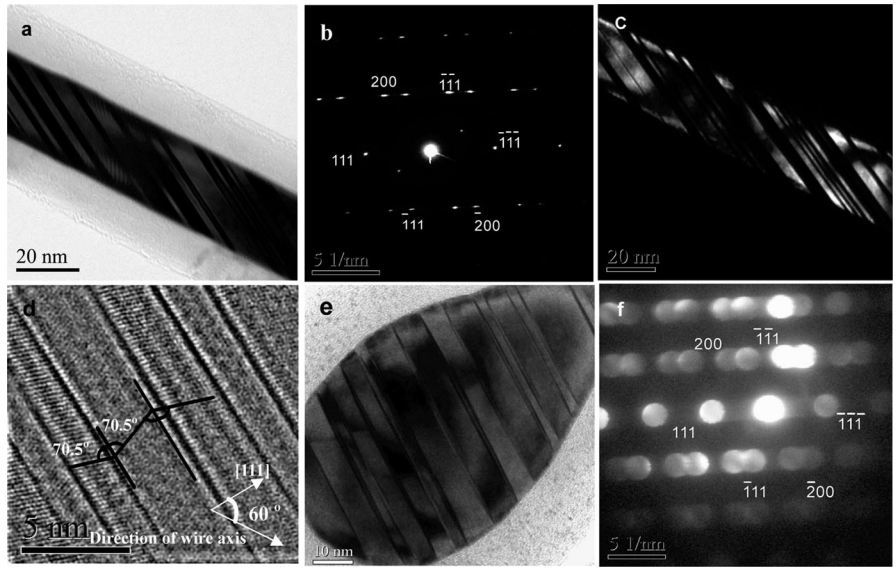

Figure 2. (a) The metal-focused bright field TEM image of a typical Co−Ni@CNT. (b) A typical SAED pattern of the Co−Ni@CNTs. (c) Dark field TEM image of the Co−Ni@CNTs. (d) HRTEM image of the sheathed Co−Ni nanowire. (e) The metal-focused TEM image of a thick end of Co−Ni@CNTs. (f) SAED pattern taken from the thick end of Co−Ni@CNTs (e).

in starting materials. Because Co and Ni are generally dissolved fully in each other over 420 °C[35,36] (much lower than the temperature of the used detonation system, about 1000 °C[34]), it is believed that the Co and Ni atoms condensed as an alloy phase. Figure 1h shows the X-ray diffraction (XRD) pattern of the produced materials. The diffraction peaks at 2θ angles of 44.5°, 51.8°, 76.4° can be assigned as face-centered cubic (fcc) nickel crystals (JCPDS 65-2865), and the peaks at 39.3°, 41.5°, 44.5°, 58.5°, 71.1°, and 77.8° assigned to hexagonal closed packed (hcp) nickel crystals (JCPDS 45-1027), suggesting that the Co−Ni alloy crystals are structured by nickel basic frameworks (note that the diffraction peaks exhibit an obvious disparity with those for cobalt crystals, as shown in Figure S4). According to the binary phase diagram of Co−Ni alloys and their physical properties, the Co−Ni alloy can form a substitutional solid solution in which the solvent and solute atoms are located randomly at the atom sites in the crystal structure of the solution. According to the XRD pattern (Figures 1h and S4), in our products, Ni can be regarded as the solvent of Co−Ni solid solution and Co is the solute. A large number of Co atoms randomly occupy atom sites of Ni crystal through substituting the Ni atoms. Certainly, this substituting process does not alter the crystalline form of Ni. Therefore, although the diffraction peaks of metal in the XRD pattern can be assigned to cubic Ni and hexagonal Ni according to the JCPDS cards, these peaks belong to Co−Ni alloy actually.

From the metal-focused TEM analyses, the Co−Ni@CNTs are imaged as high-density light/dark segments throughout the entire length, as shown in Figure 2a,c, and e typically, associated with lamellar twin structures. Selective area electron diffraction (SAED) (Figure 2b and f) confirms that the Co−Ni alloy nanowires have the (111) twinned structure, commonly appearing in the fcc structured crystals.[12,24] HRTEM images, as shown in Figure 2d, additionally display the zigzag structural feature of lamellar twins. The zigzag angles are 141° (70.5° + 70.5°), in good agreement with the theoretical estimation of the relative rotational angle of the (111) twin crystals in (fcc) structures.[24,26,37] The twinned Co−Ni nanowires have high-density twinning boundaries, characterized by the small distance between two adjacent boundaries, in the range of 1.0−12 nm, peaked at about 4 nm. Note that in the present twinned Co−Ni nanowires, there

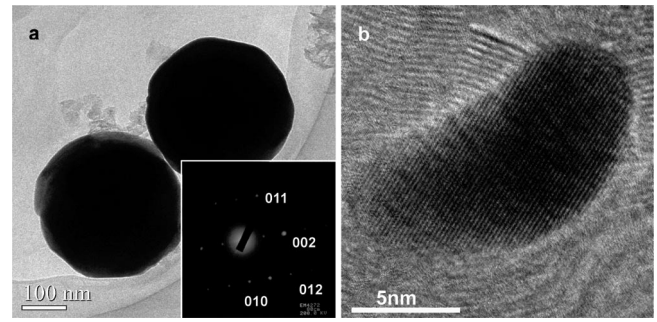

Figure 3. (a) TEM image of Co−Ni alloy particles. Inset: SAED pattern of the right particle. (b) HRTEM image of a small Co−Ni alloy nanoparticle.

is an angle of about 60° between the [111] direction (perpendicular to (111) twin boundary) and the wire axis. It is much different from the situation of the common (111) twin nanowires reported by other authors,[3,12,23,24] where the nanowires grow in the [111] direction following the vapor−liquid−solid model,[3,12,23,24] implying that the formation of the present Co−Ni@CNTs might comply a different mechanism.

From TEM and SAED analyses, all of the Co−Ni alloy nanowires sheathed inside CNTs exhibit cubic twinned structures. It appears to somewhat disagree with the XRD results, which also show the presence of hexagonal structures (Figure 1h). Using TEM and SAED, we find that the hexagonal structures actually derive from the small amount of Co−Ni alloy particles (Figure 3a). SAED results unambiguously reveal that some of the particles exhibit a hexagonal single crystal structure (inset of Figure 3a) and some of them have an fcc structure (not shown), possibly resulted from different local environments. More interestingly, the Co−Ni alloy particles are all single crystals as revealed by both SAED (Figure 3a) and HRTEM (Figure 3b) independent of stacking structure, which sharply contrasts with the situation of the Co−Ni@CNTs. This observation implies that the narrow channels of CNTs might display a confinement effect on the formation of lamellar twins in the Co−Ni alloy nanowires. To give insight into the confinement effect of CNTs, it is necessary to first understand the formation mechanism of the Co−Ni@CNTs.

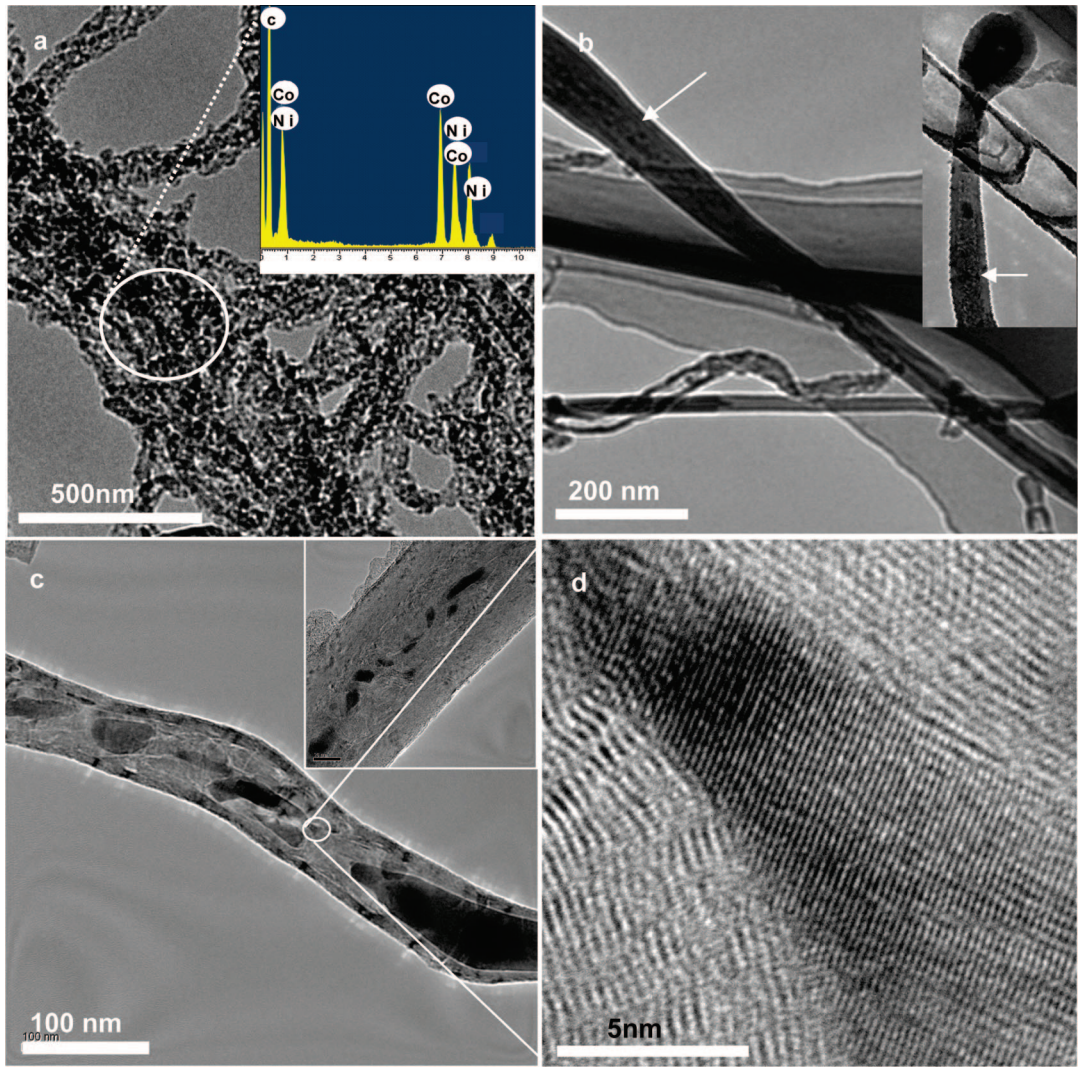

Figure 4. (a) TEM image of the materials obtained by freezing the synthesis system. Inset: EDX spectrum of the materials. (b) TEM image of a frozen semideveloped Co−Ni@CNT. The inset shows a similar one. All show that part of the metals has been developed into continuous wires while part of them (arrowed) still remains as particles. (c) A magnified TEM image of a frozen semideveloped Co−Ni@CNT, in which metals are present as particles. (d) HRTEM image of the small Co−Ni alloy nanoparticle wrapped in CNT.

It is believed that the formation of the Co−Ni@CNTs is closely linked with the formation of CNTs. About the formation of CNTs in the presence of metal catalysts, a frequently cited mechanism is the adsorption−diffusion−deposition (ADP) model,[38−41] which is based on the observation that one metal particle is often located at one of the two tube ends. This model obviously fails to explain the formation of the present CNTs fully filled with Co−Ni alloy nanowires. Recently, we reported that for the vapor deposition processes with in situ-formed metal catalysts (including the DACVD employed here), the formation of CNTs follows a particle−wire−tube (PWT) stepwise evolution mechanism.[42] We preliminarily estimate that the formation of the present Co−Ni@CNTs might follow a similar way. To get a better understanding, we have frozen possible evolution intermediates by quickly decreasing system temperature (see Experimental Methods). Some typical intermediates are shown in Figure 4. Most of the intermediates exhibit wirelike morphology and are obviously assembled by particles (Figure 4a), which contain a large amount of cobalt and nickel as revealed by EDX analysis (inset of Figure 4a). In wires, cobalt and nickel are present in very small size, embedded in carbon matrixes. Some intermediates have developed into tubular structures, inside which grown metal particles are evident but still isolated (Figure 4b,c, including the insets). As was revealed by HRTEM analyses, the particles exhibit a single-crystal structure (Figure 4d). Figure 4b additionally displays that within a single tube, part of the metals are present as continuous nanowires, while part of them still remain as isolated particles. These observations suggest that the evolution of the Co−Ni alloy nanowires is the natural consequence of a fusion of the small metal nanoparticles. About the fusion behavior of metal particles, we have further observed in situ by TEM, as shown in Figure S5. Under electron beam irradiation, two isolated Co−Ni alloy particles embedded in carbon matrix (involved in the frozen 1D assembly) tend to move close to each other and fuse together, with increasing irradiation time. From the information described above, we deduce that the formation of Co−Ni@CNTs follows a stepwise evolution process: Co−Ni alloy particles coated with carbons are first formed and then self-organize into 1D assemblies (driven by anisotropic interaction), which finally transform into CNT-sheathed continuous Co−Ni alloy nanowires via the fusion of the metal particles, accompanied by the formation and crystallization of CNT walls. It has been well-known that fully closed and graphitized spherical particles are nearly isotropic and thus difficult to assemble orientationally. However, the incipiently formed carbon nanoparticles (including the metal-

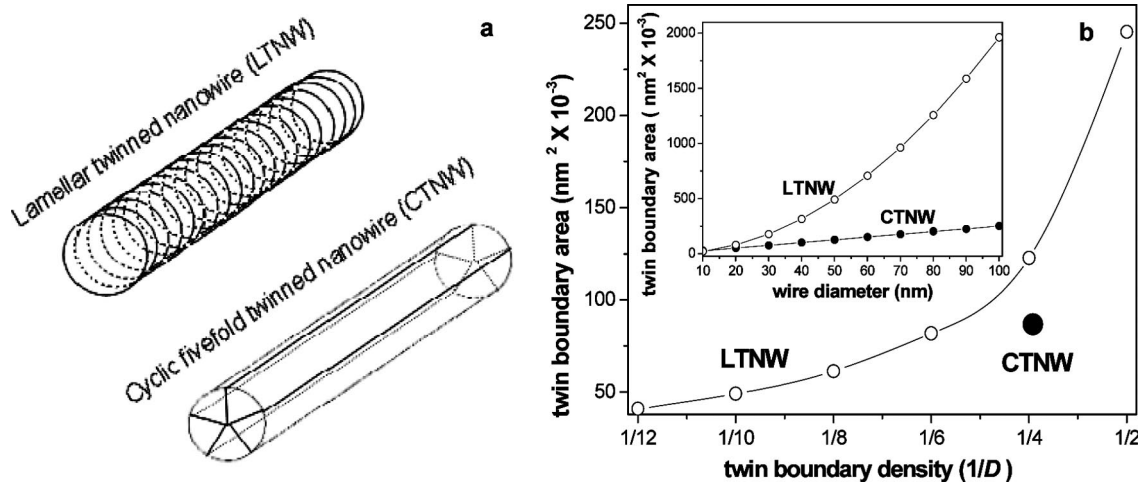

Figure 5. (a) Schematic model of cyclic 5-fold twinned nanowire (CTNW) and lamellar twinned nanowire (LTNW). (b) The twin boundary area as a function of twin boundary density for LTNW for a given nanowire with diameter of 25 nm and length of 1000 nm. The round black spot indicates the value for CTNW with the same dimensions. The inset is twin boundary area as a function of wire diameter for LTNW (boundary density $1/D = 0.25$) and CTNW for a given nanowire with length of 1000 nm.

filled particles) during the deposition of carbon species exhibit ill-crystallized layered structures. Such structures are far from graphitized and have lots of defects (such as sp^3 carbons, nonhexagonal rings, disconnected bonds, etc.),[43] especially at the two edges of the around-curved carbon (not graphite) layers, which would endow the layered structures strong anisotropy. Under proper conditions, the defective layered structures might assemble by defect−defect interactions, lip−lip interactions,[44] and possible metal−carbon conjugations.[45] During the assembling, an anisotropy-induced dipole−dipole interaction and the defect−defect interaction between the defective and anisotropic nanoparticles likely give the primary driving forces.

Such an evolution mechanism of Co−Ni@CNTs gives rich information for the understanding of the formation of the high-density lamellar twin boundaries in the sheathed Co−Ni alloy nanowires. As described above, the Co−Ni alloy nanowires are formed via the fusion of Co−Ni alloy particles, which naturally gives a topological choice for the formation of lamellar twins. In the present process, the alloy particle fusion and the nanowire crystallization are confined inside the closed and narrow channels of CNTs, and the energy generated from the fusion and crystallization is difficult to release from the local environment due to the limited thermal conductivity of the layered CNT walls. Additionally, the formation of alloy nanowires and the crystallization of CNT walls occur at nearly the same time, and the energy released from the crystallization of CNT walls will be partially confined inside CNT channels. Therefore, the confined energy makes the tube-channel-encapsulated metals stay at a high energy state and thus result in a kinetic control of the formation and crystallization of the alloy nanowires. In the confined kinetic environment, high-density twinning boundaries are formed to effectively store and reduce the energy and to make the alloy nanowires stable quickly. Additionally, in the present system, the high content of metals and the confining effect of carbon nanotube channels predictable make the metals exhibit an extremely high supersaturated state. The supersaturation would lead to a high chemical potential, which make the difference in nucleation barriers for ordinary and twin nucleus very small and thus facilitate the formation of twin planes.[3] Considering the energy storage and reduction, the formation of high-density lamellar twins is more efficient than the formation of cyclic 5-fold twins because the total boundary area of lamellar twin is much higher than that of cyclic 5-fold twin when the lamellar twin boundary has a high density (Figure 5a). For example, for a given cylindrical nanowire (diameter, 25 nm; length, 1000 nm) with a density of lamellar twin boundary $1/D$ (D, the distance between two adjacent boundaries) of 0.25, a situation similar to the Co−Ni nanowire described here, the total area of twinning boundary is 122 656 nm^2, which is about 2 times larger than the area (62 500 nm^2) for a cyclic 5-fold twinned nanowire with the same diameter and length (Figure 5b). Note that the difference in the total area of twinning boundary will be higher with increasing wire diameter (inset of Figure 5b). As a conclusion, the formation of high-density lamellar twinning structures in the CNT-sheathed Co−Ni alloy nanowires is likely the consequence of the confinement function of CNTs. Similar structures have been observed in the CNT-sheathed nanowires of pure metals such as iron and cobalt (Figure S6).

4. Conclusions

In summary, carbon nanotube-sheathed Co−Ni alloy nanowires have been fabricated by detonation-assisted chemical vapor deposition. The Co−Ni alloy nanowires are formed from the fusion and crystallization of Co−Ni alloy nanoparticles. Unlike previously reported metal nanowires, the present Co−Ni nanowires contain high-density lamellar twinned boundaries, which are kinetically produced by a confinement function of the closed and narrow channels of CNTs. This new knowledge may scientifically provide valuable information for a better understanding of twin formation and technically lead to a designed crystallization control of inorganic nanowires. In addition, the unique characteristic of the CNT-sheathed Co−Ni alloy nanowires may be applicable in nanoelectronic devices, data storage, sensors, and microscopic probes (especially in magnetic force microscopy).

Acknowledgment. This work is financially supported by NSFC (Nos. 20673135, 20473109, 50534100) and CAS following the "Bairen" program. We gratefully thank Prof. Yutian Shen (Tsinghua University), Prof. Guoqing Gui (Institute of Coal Chemistry of CAS), and Prof. Jingbo Li (Institute of Physics of CAS) for their valuable discussion and help in sample analyses.

Supporting Information Available: Figures S1−S6. This material is available free of charge via the Internet at http://pubs.acs.org.

References and Notes

(1) Tian, M.; Wang, J.; Kurtz, J.; Mallouk, T. E.; Chan, M. H. W. *Nano Lett.* **2003**, *3*, 919.
(2) Cui, Y.; Zhong, Z.; Wang, D.; Wang, W. U.; Lieber, C. M. *Nano Lett.* **2003**, *3*, 149.
(3) Johansson, J.; Karlsson, L. S.; Patrik, T. S. C.; Martensson, T.; Wacaser, B. A.; Deppert, K.; Samuelson, L.; Seifert, W. *Nat. Mater.* **2006**, *5*, 574.
(4) Cho, K. S.; Talapin, D. V.; Gaschler, W.; Murray, C. B. *J. Am. Chem. Soc.* **2005**, *127*, 7140.
(5) Cao, H.; Xu, Z.; Sang, H.; Sheng, D.; Tie, C. *Adv. Mater.* **2001**, *13*, 121.
(6) Yin, A. J. *Appl. Phys. Lett.* **2001**, *79*, 1039.
(7) Wang, J.; Huang, H. *Appl. Phys. Lett.* **2006**, *88*, 203112.
(8) Wang, J.; Tian, M.; Mallouk, T. E.; Chan, M. H. W. *J. Phys. Chem. B* **2004**, *108*, 841.
(9) Zhang, X. *Appl. Phys. Lett.* **2004**, *84*, 1096.
(10) Lu, L.; Shen, Y.; Chen, X.; Qian, L.; Lu, K. *Science* **2004**, *304*, 422.
(11) Ikonic, Z.; Srivastava, G. P.; Inkson, J. C. *Surf. Sci.* **1994**, *307*−*309*, 880.
(12) Xiong, Q.; Wang, J.; Eklund, P. C. *Nano Lett.* **2006**, *6*, 2736.
(13) van Bueren, H. G. *Imperfections in Crystals*; North-Holland Publishing Co.: North-Holland, 1961.
(14) Marks, L. D. *Rep. Prog. Phys.* **1994**, *57*, 603.
(15) Johnson, C. J.; Dujardin, E.; Davis, S. A.; Murphy, C. J.; Mann, S. *J. Mater. Chem.* **2002**, *12*, 1765.
(16) Lisiecki, I.; Filankembo, A.; Sack-Kongehl, H.; Weiss, K.; Pileni, M. P.; Urban, J. *Phys. Rev. B* **2000**, *61*, 4968.
(17) Zhang, S. H.; Jiang, Z. Y.; Xie, Z. X.; Xu, X.; Huang, R. B.; Zheng, L. S. *J. Phys. Chem. B* **2005**, *109*, 9416.
(18) Chen, H.; Gao, Y.; Yu, H.; Zhang, H.; Liu, L.; Shi, Y.; Tian, H.; Xie, S.; Li, J. *Micron* **2004**, *35*, 469.
(19) Wu, B.; Heidelberg, A.; Boland, J. J.; Sader, J. E.; Sun, X.; Li, Y. *Nano Lett.* **2006**, *6*, 468.
(20) Sun, X.; Li, Y. *Adv. Mater.* **2005**, *17*, 2626.
(21) Sun, Y. G.; Mayers, B.; Herricks, T.; Xia, Y. N. *Nano Lett.* **2003**, *3*, 955.
(22) Shen, G.; Bando, Y.; Liu, B.; Tang, C.; Golberg, D. *J. Phys. Chem. B* **2006**, *110*, 20129.
(23) Bhunia, S.; Kawamura, T.; Fujikawa, S.; Nakashima, H.; Furukawa, K.; Torimitsu, K.; Watanabe, Y. *Thin Solid Films* **2004**, *464*, 244.
(24) Hao, Y.; Meng, G.; Wang, Z. L.; Ye, C.; Zhang, L. *Nano Lett.* **2006**, *6*, 1650.
(25) Li, Q.; Gong, X.; Wang, C.; Wang, J.; Ip, K.; Hark, S. *Angew. Chem., Int. Ed* **2002**, *41*, 3489.
(26) Chen, H.; Wang, J.; Yu, H.; Yang, H.; Xie, S.; Li, J. *J. Phys. Chem. B* **2005**, *109*, 2573.
(27) Elechiguerra, J. L.; Reyes-Gasga, J.; Yacaman, M. J. *J. Mater. Chem.* **2006**, *16*, 3906.
(28) Molares, M. E. T.; Buschmann, V.; Dobrev, D.; Neumann, R.; Scholz, R.; Schuchert, I. U.; Vetter, J. *Adv. Mater.* **2001**, *13*, 5.
(29) Wang, J.; Huang, H.; Kesapragada, S. V.; Gall, D. *Nano Lett.* **2005**, *5*, 2505.
(30) Sauer, G. *J. Appl. Phys.* **2002**, *91*, 3243.
(31) Lu, Y.; Zhu, Z.; Wu, W.; Liu, Z. *Carbon* **2003**, *41*, 194.
(32) Lu, Y.; Zhu, Z.; Wu, W.; Liu, Z. *Chem. Commun.* **2002**, 2740.
(33) Lu, Y.; Zhu, Z.; Liu, Z. *Carbon* **2004**, *42*, 361.
(34) Zhu, Z.; Su, D.; Lu, Y. I.; Schlogl, R.; Weinberg, G.; Liu, Z. *Adv. Mater.* **2004**, *16*, 443.
(35) *Constitution of Binary Alloys, Metallurgy and Metallurgical Engineering Series*; McGraw-Hill Book Co.: New York, 1958.
(36) Tury, B.; Lakatos-Varsanyi, M.; Roy, S. *Surf. Coat. Technol.* **2006**, *200*, 6713.
(37) Xiong, Q.; Wang, J.; Eklund, P. C. *Nano Lett.* **2006**, *6*, 2736.
(38) Amelinckx, S.; Zhang, X. B.; Bernaerts, D.; Zhang, X. F.; Ivanov, V.; Nagy, J. B. *Science* **1994**, *265*, 635.
(39) Liu, L.; Fan, S. *J. Am. Chem. Soc.* **2001**, *123*, 11502.
(40) Lee, C. J.; Park, J. *J. Phys. Chem. B* **2001**, *105*, 2365.
(41) Charlier, J. C.; De Vita, A.; Blase, X.; Car, R. *Science* **1997**, *275*, 647.
(42) Du, G.; Feng, S.; Zhao, J.; Song, C.; Bai, S.; Zhu, Z. *J. Am. Chem. Soc.* **2006**, *128*, 15405.
(43) Charlier, J. C. *Acc. Chem. Res.* **2002**, *35*, 1063.
(44) Kwon, Y. K.; Lee, Y. H.; Kim, S. G.; Jund, P.; Tománek, D.; Smalley, R. E. *Phys. Rev. Lett.* **1997**, *79*, 2065.
(45) Deng, W. Q.; Xu, X.; Goddard, W. A. *Nano Lett.* **2004**, *4*, 2331.

JP804380X